Applied Physics Letters

Temperature-dependent mechanical behavior of an $Al_{0.5}Cr_{0.9}FeNi_{2.5}V_{0.2}$ high-entropy alloy

Cite as: Appl. Phys. Lett. **119**, 121902 (2021); https://doi.org/10.1063/5.0064821
Submitted: 27 July 2021 • Accepted: 07 September 2021 • Published Online: 21 September 2021

Shichao Zhou, Peter K. Liaw, Yunfei Xue, et al.

Applied Physics Letters ARTICLE scitation.org/journal/apl

Temperature-dependent mechanical behavior of an $Al_{0.5}Cr_{0.9}FeNi_{2.5}V_{0.2}$ high-entropy alloy

Cite as: Appl. Phys. Lett. **119**, 121902 (2021); doi: 10.1063/5.0064821
Submitted: 27 July 2021 · Accepted: 7 September 2021 ·
Published Online: 21 September 2021

Shichao Zhou,[1,a)] Peter K. Liaw,[2,b)] Yunfei Xue,[3,c)] and Yong Zhang[1,4,5,d)]

AFFILIATIONS

[1]Beijing Advanced Innovation Center of Materials Genome Engineering, State Key Laboratory for Advanced Metals and Materials, University of Science and Technology Beijing, 30 Xueyuan Road, Beijing 100083, China
[2]Department of Materials Science and Engineering, The University of Tennessee, Knoxville, Tennessee 37996, USA
[3]School of Materials Science and Engineering, Beijing Institute of Technology, Beijing 100081, China
[4]Shunde Graduate School of University of Science and Technology Beijing, Foshan 528399, China
[5]Qinghai Provincial Key Laboratory of New Light Alloys, Qinghai University, Xining 810016, China

Note: This paper is part of the APL Special Collection on Metastable High Entropy Alloys.
[a)]**Electronic mail:** shichaozhou6@163.com
[b)]**Electronic mail:** pliaw@utk.edu
[c)]**Electronic mail:** xueyunfei@bit.edu.cn
[d)]**Author to whom correspondence should be addressed:** drzhangy@ustb.edu.cn

ABSTRACT

High-entropy alloys (HEAs) with a ductile face-centered-cubic matrix and coherent nano-precipitates ($L1_2$) are promising candidate materials for heat-resistant applications. In the present work, we systematically investigated the mechanical behavior of a wrought $L1_2$-type-strengthened HEA, $Al_{0.5}Cr_{0.9}FeNi_{2.5}V_{0.2}$, at elevated temperatures ranging from 500 to 900 °C. We find that the $Al_{0.5}Cr_{0.9}FeNi_{2.5}V_{0.2}$ HEA shows a moderate strength (~875 MPa) as well as ductility (~15%) at 500 °C and then a distinct ductile-to-brittle transition at 600 °C due to the brittle body-centered-cubic phase and weak deformation accommodation at grain boundaries (GBs). The further increase in temperatures up to 850 °C caused a decrease in strength but an increase in ductility owing to the occurrence of dynamic restoration. Correspondingly, kernel average misorientation maps of specimens exhibited a strain concentration along GBs and different deformation accommodation abilities under various conditions.

High-entropy alloys (HEAs) have opened up a new age in high-performance materials for structural applications because multi-principal elements strategy can overcome the strength–ductility trade-off easier than traditional alloys.[1–9] To date, HEAs can be classified simply by preparation processes, casting HEAs (such as $Al_{19}Fe_{20}Co_{20}Ni_{41}$[8]), deformed HEAs ($Al_{0.3}CoCrFeNi$,[6] we can name it as GS101), and film and coating HEAs [$(Al_{0.5}CrFeNiTi_{0.25})N_x$[7]]. Among them, the deformed HEAs with the face-centered-cubic (FCC) matrix strengthened by coherent nano-precipitates ($L1_2$ phase) have attracted much attention owing to their ductile nature that the ductile FCC matrix, nano-$L1_2$ precipitates, and coherent interfaces between them can promote an excellent balance between strength and ductility at room and cryogenic temperatures.[10–15] For example, Yang *et al.*[12] prepared a $(FeCoNi)_{86}Al_7Ti_7$ HEA with high-density $L1_2$ nano-precipitates, which exhibited both high tensile strength (~1.5 GPa) and ductility (~50%) at ambient temperature. On the other hand, Tong *et al.*[15] found a $FeCoNiCrTi_{0.2}$ HEA strengthened by $L1_2$ nano-precipitates possessed excellent tensile strength (~1.5 GPa) and ductility (~46%) at 77 K. Furthermore, in consideration of the microstructures, FCC/$L1_2$, similar to Ni-based superalloys (a γ matrix and γ' precipitates), this type of HEAs is promising potential structure materials for elevated-temperature applications.[16] However, to date, there are few studies about the mechanical behavior of FCC/$L1_2$ HEAs at elevated temperatures. For example, Yang *et al.*[16] investigated the mechanical property of the Ni-30Co-13Fe-15Cr-6Al-6Ti-0.1B (in at. %) HEA with different aging processes at 700 °C and revealed the formation mechanism of Heusler phases at grain boundaries (GBs). Moreover, Chang and Yeh[17] and Kuo and Tsai[18] investigated the formation of cellular precipitates at GBs and its effect on mechanical properties from room temperature to 1000 °C. These studies about

mechanical behavior at elevated temperatures focused on small-size specimens with about 50 g and then the cold-rolled process. However, the forging process is significant for $L1_2$-type strengthened HEAs with kilograms degree, which is similar to wrought Ni-based superalloys that are the most widely used among all types of Ni-based superalloys.[19,20] Moreover, the forging process can break through the limit of rolling deformation and further promote the development of HEAs. The $Al_{0.5}Cr_{0.9}FeNi_{2.5}V_{0.2}$ HEA[13,14] with a high Ni/Al ratio can promote the formation of high-density Ni_3Al-type $L1_2$ phases, which contributes to high strength and excellent ductility at elevated temperatures. However, the mechanical behavior and underlying deformation mechanism at high temperatures have not been studied. Thus, in the present work, we systematically investigated the mechanical behavior of a wrought $L1_2$-type strengthened HEA with kilograms, $Al_{0.5}Cr_{0.9}FeNi_{2.5}V_{0.2}$, at elevated temperatures from 500 to 900 °C.

The $Al_{0.5}Cr_{0.9}FeNi_{2.5}V_{0.2}$ HEA was prepared by vacuum-induction melting with high-purity raw materials (~99.9 wt. %) in an argon atmosphere. Subsequently, an ingot with 2 kg was produced by wire-based electrical discharge machining [Fig. 1(a)], followed by a solid solution treated at 1200 °C for 24 h, then subjected to multi-pass forged to ~67% reduction in diameter (the diameter reduced from 60 to 20 mm) at 1200 °C, and finally cooled in the air [Fig. 1(b)]. By highly alloying with the Al addition, plenty of nanoscale $L1_2$ nano-precipitates were introduced in this alloy within the cooling process. Thus, the subsequent aging process was not conducted. Microstructures and morphologies of specimens with wrought and tensile tests at different temperatures were characterized by a Zeiss Supra 55 field emission scanning electron microscope (SEM) equipped with an electron back-scattering diffraction (EBSD) system. The EBSD specimens were mechanically ground by a 2500-grit SiC paper, followed by electro-chemically polishing with a mixture of 80% ethanol and 20% perchloric acid (vol. %) at room temperature. The kernel average misorientation (KAM) angle within the grains was measured by the Aztec software. Dumbbell-shaped tensile specimens with a gauge length of 18 mm and diameter of 3 mm were machined from the forged bar. The uniaxial tensile tests were performed with a DDL50 tensile machine at the temperatures ranging from 500 to 900 °C with an initial strain rate of 5×10^{-5} s^{-1} and then increased to 3×10^{-3} s^{-1} after yielding. Three specimens were measured to confirm the reproducibility, and representative engineering stress–strain curves were plotted.

Figures 1(a) and 1(b) show the initial HEA ingot with 60 mm and the forged bar with 20 mm in diameter after multi-pass forging, respectively. Figure 1(c) presents plenty of $L1_2$ nano-precipitates in the grain interiors, which is consistent with previous studies.[13,14] Figure 1(f) shows the grain-size distributions of hierarchical grains quantitatively. The wrought microstructure consists of coarse grains (an average size of ~244 μm) around refined grains (an average size of ~53 μm), indicating a typical mixed grain structure, as shown in Figs. 1(d) and 1(e). The grain-size heterogeneity can be attributed to dynamic recrystallization during the forging process at 1200 °C.[21] Moreover, the typical annealing twins are observed within grain interiors.

Representative engineering stress–strain curves of the tensile tests at different temperatures are shown in Fig. 2(a). It is found that the failure strain gradually decreases first at temperatures ranging between 500 and 800 °C and then increases at above 850 °C. It also can be classified as three temperature regimes with markedly different tensile ductility. First, at a low temperature (500 °C), this HEA remains ductile with a failure strain of about 15%. Second, a significant reduction in tensile ductility is observed at a mid-temperature between 600 and 850 °C, with a negligible tensile ductility of below 3%. Third, a high-temperature regime at 900 °C where ductility is restored. Figure 2(b) shows corresponding specimens after the tensile tests in the temperature range of 500–900 °C, which are consistent with the trend of tensile ductility. The dramatic loss in ductility between 600 and 850 °C is similar to studies for other HEAs[16–18,22] and Ni-based superalloys.[20] Such a phenomenon is termed as the intermediate temperature embrittlement, which means that the maximum elongation or reduction in area at intermediate temperatures is much lower than those at low and high temperatures in tensile tests.[20] The sudden and rapid fracture along GBs in the tensile process, especially near the yielding

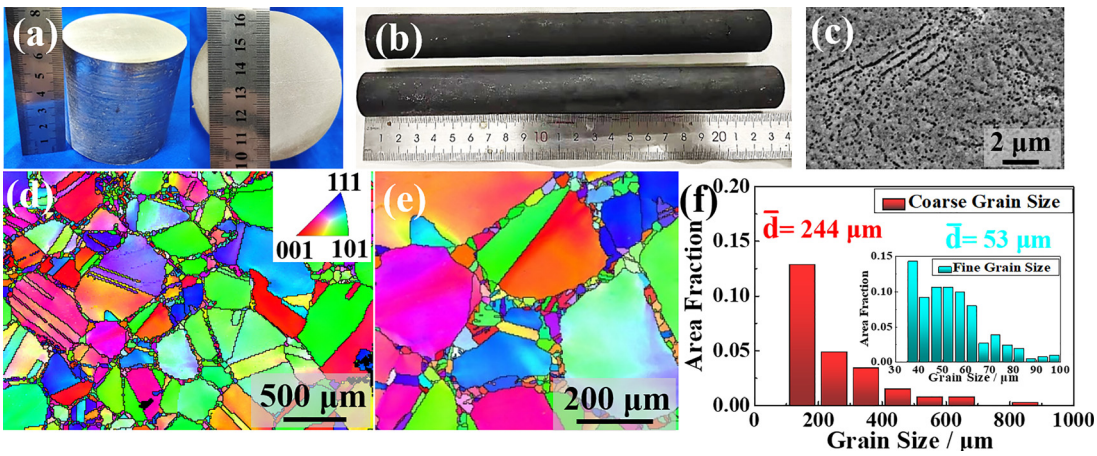

FIG. 1. (a) $Al_{0.5}Cr_{0.9}FeNi_{2.5}V_{0.2}$ HEA ingot with a diameter of 60 mm. (b) Forged bar with a diameter of 20 mm after the multi-pass forging process at 1200 °C. (c) Plenty of $L1_2$ nano-precipitates in the grain interiors. (d) and (e) EBSD mapping showing a microstructure and morphology with mixed grains. (f) Coarse and fine grains size distributions of this HEA, respectively.

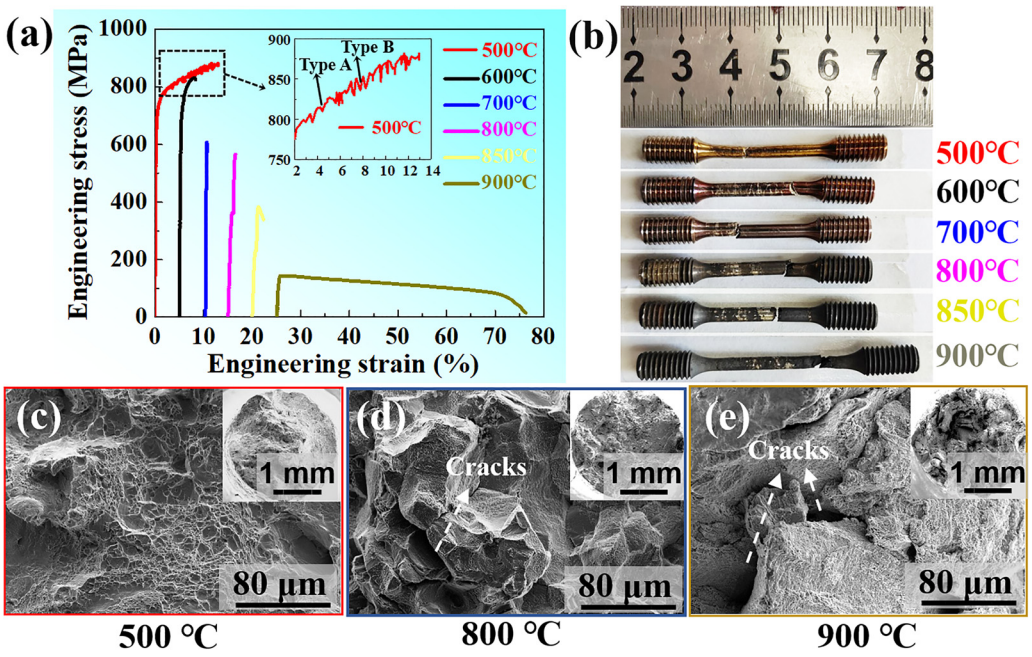

FIG. 2. (a) Engineering stress–strain curves of the $Al_{0.5}Cr_{0.9}FeNi_{2.5}V_{0.2}$ HEA tested from 500 to 900 °C in air and (b) corresponding specimens after tensile tests. (c)–(e) Representative SEM fractographs of this HEA tested at 500, 800, and 900 °C, respectively.

point, is one of the most severe limits for their practical applications at elevated temperatures. The corresponding mechanism of the mediate–intermediate temperature embrittlement would be discussed in the next section. It is evident that the flow stresses present a strain hardening until failure at all temperatures except 850 and 900 °C, at which stresses achieve a peak value and then decrease gradually. The flow-stress softening may be attributed to the dynamic recovery and recrystallization during the plastic deformation process at higher temperatures (850 and 900 °C).[23] Both the yield and ultimate strengths decrease gradually with the increase in temperatures as normal.[24] Among them, the specimens tested at 500 °C exhibit the high tensile strength (~875 MPa) and excellent fracture ductility (~15%). Moreover, it is well worth noticing that the yield strength presents an anomalous increase in the temperature range from 500 to 600 °C, which could be attributed to the activation of multiple slip systems at the peak yielding temperature (600 °C).[25] As a result, the formation of Kear–Wilsdorf locks is promoted, which could hinder the movement of dislocations and lead to anomalous yield and hardening.[26,27] In addition, in contrast to smooth curves above 600 °C, serrations are observed at 500 °C from the inset [Fig. 1(a)]. As we all know, there are three typical types of serrations, namely, Types A, B, and C. Type A serrations represent a sparse distribution on the stress–strain curve and smaller stress drop, followed by an abrupt rise of stress. Type C serrations are characterized by a denser distribution and lager range of stress drop. One in-between is Type B. According to the inset from Fig. 2(a), representative type (A+B) serrations are observed, which can be ascribed to dynamic strain aging (DSA) that interacts between solute-atoms diffusion and movable dislocations movement.[28,29]

Given the similar tensile behaviors in the tested temperature range between 600 and 850 °C, for clarity and simplicity, we will mainly focus on analysis and discussion at three representative temperatures, namely, 500, 800, and 900 °C. Figures 2(c) and 2(d) show a distinct ductile-to-brittle transition with a fully ductile rupture surface dominated by dimples and a typical brittle intergranular fracture characterization accompanied by cleavage facets at 500 and 800 °C, respectively. Thus, between 600 and 850 °C, the negligible tensile ductility can be attributed to the detrimental intergranular embrittlement, which was clearly demonstrated from the fractured surfaces consisting of numerous cleavage facets and intergranular cracks, as shown in Fig. 2(d). Meanwhile, it is interesting to note that Fig. 2(e) also shows an intergranular fracture characterization owing to intergranular cracks along GBs,[24] though its ductility beyond 50% at 900 °C. The results presented above demonstrate conclusively that the $Al_{0.5}Cr_{0.9}FeNi_{2.5}V_{0.2}$ HEA is prone to intergranular embrittlement between 600 and 850 °C.

In order to reveal the intergranular embrittlement fracture mechanism, further microstructure observations focusing on GBs were performed by back-scattering diffraction (BSD) with high magnification and EBSD. The needle-shaped and blocky intergranular phases are observed by SEM at specimens after a forged process, as displayed in Fig. 3(a). Both studies[13,14] and further detailed analyses with EBSD reveal that the phases along GBs are a body-centered-cubic (BCC) structure, as characterized in Fig. 3(b). Similarly, such a BCC phase was also observed in other HEAs strengthened by $L1_2$, for example, $(FeNiCoCr)_{1-x-y}Al_xTi_y$,[10,11] $Co_{30}Ni_{29.9}Cr_{15}Fe_{13}Al_6Ti_6B_{0.1}$,[16] and $(FeCoNi)_{86}Al_7Ti_7$.[12] Previous studies[13,14] revealed that the BCC phase is prone to formation at intermediate temperatures. Thus, we speculate that this BCC phase formed during the cooling stage in air after a forged process. This kind of a BCC phase is not only brittle but also incoherent with the FCC matrix.[10] This means that the formation of such BCC phases, especially at GBs, may lead to an increase in the

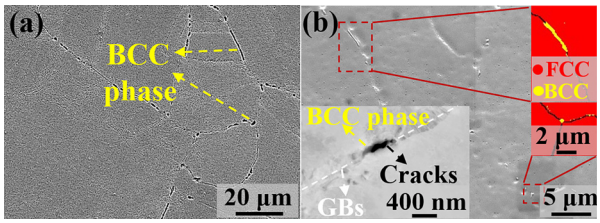

FIG. 3. Representative (a) SEM and (b) EBSD micrographs of specimens after a forged process showing the distribution of a needle-shaped and blocky BCC phase at GBs. Left inset from (b) showing cracks initiated from the BCC phase at GBs with a back-scattering diffraction (BSD) mode at 800 °C.

local stress concentration and then brittle alloys.[16] Previous studies[30,31] revealed that minor amounts of such BCC phases at the GBs may be little harmful for tensile properties at ambient temperature. However, it could result in a serious intergranular embrittlement fracture at the intermediate temperatures for alloys enriched with Ni. Therefore, the detrimental brittle intermetallic BCC phases along GBs are considered to cause mechanical property degradation, especially for ductility, by acting as sites for cracks nucleation.[32] Subsequently, cracks propagate along with the interface of the BCC phase and matrix, resulting from significant deformation incompatibility.[17,18] Consequently, the main crack consisting of nearby cracks formed along boundaries, leading to intergranular rapture at an early stage of plastic deformation during tensile tests.[20] The left inset of Fig. 3(b) confirms this viewpoint that cracks initiate and propagate along with the interface between the BCC phase and matrix at GBs. Furthermore, the formation of BCC phases usually depletes some elements from the matrix, resulting in a weakening effectiveness for solid-solution strengthening.[16] Furthermore, a mixed microstructure consisting of refined and coarse grains provides major amounts of GBs for the nucleation of BCC phases and cracks, which further promoted ductility degradation. Thus, the formation of BCC phases causes degeneration of both strength and ductility, especially at intermediate temperatures.

In order to characterize the strain distribution in the matrix at various deformation temperatures, EBSD measurements as well as values of kernel average misorientation (KAM) of fractured specimens at various test temperatures were achieved. KAM is the average misorientation among all adjoining pixels, which is used to assess the local strain and reflect qualitatively the density of geometrically necessary dislocations (GNDs) for crystalline materials.[33] Compared with interiors of grains, relatively higher KAM values can be observed near the GBs especially at the intergranular cracks, implying a strain concentration and a larger density of GNDs concentrate at GBs, as displayed in Figs. 4(c)–4(e). During plastic deformation, the deformation compatibility among vicinity grains can be attributed to the accumulation of dislocations and slip-assisted GB sliding.[19,34] The GBs are considered as an obstacle in the slipping of dislocations and then promote the pileup of dislocations, resulting in the strain concentration at the GBs. Furthermore, in comparison with the specimen deformed at 800 °C, the counterparts tested at 500 and 900 °C exhibited higher KAM values, which means a larger local strain concentration. Moreover, the relative fraction of the KAM angles at various temperatures is summarized quantitatively in Fig. 4(f) accordingly. It can be clearly observed that the specimen tested at 800 °C is dominated by a low KAM angle (below 0.3°) and elevated angle (about 0.5°) at 500 and 900 °C,

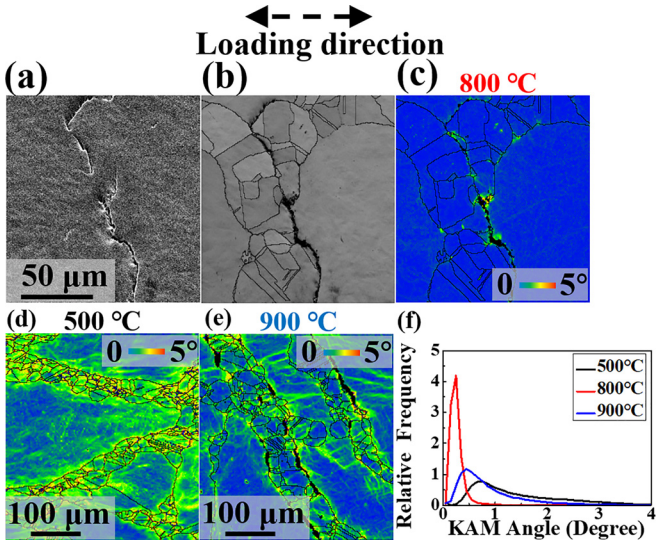

FIG. 4. Longitudinal section morphologies and kernel average misorientation (KAM) maps of specimens after tensile fracture at 500, 800, and 900 °C. (a) Intergranular cracks image and (b) corresponding band contrast map at 800 °C. (c)–(e) KAM maps showing the serious localized stress concentration at the GBs and associated crack propagation along with them at 800, 500, and 900 °C, respectively. (f) Distributions of KAM angles at various temperatures.

respectively. It implies that GBs are capable of accommodating the strain at 500 and 900 °C but not able to withstand minor amounts of local strains and dislocations pileups between 600 and 850 °C. In addition, as discussed above, intergranular BCC phases further promote strain concentration and lead to crack along GBs. Thus, the detrimental intergranular embrittlement fracture is attributed to the collective effect by BCC phases along GBs and the weak coordination deformation accommodation ability. When the deformation temperature exceeded 850 °C, the ductility recovery is ascribed to an increase in GBs mobility and dynamic restoration. Furthermore, at the peak temperature of 900 °C, the ability to relieve local stresses at GBs increases with the increase in temperature, resulting in the maximum tensile ductility (~50%).[19]

In summary, the tensile-mechanical behavior of the wrought $L1_2$-strengthened $Al_{0.5}Cr_{0.9}FeNi_{2.5}V_{0.2}$ HEA with hierarchical structures was studied between 500 and 900 °C.

(1) This HEA exhibits a moderate strength (~875 MPa) and ductility (~15%) at 500 °C due to plenty of ductile $L1_2$ phases and good coordination of GBs.
(2) Intermediate temperature embrittlement prefers to occur along GBs owing to brittle BCC phases and deformation compatibility among vicinity grains at the deformation temperature ranging from 600 and 850 °C.
(3) Moreover, dynamic recrystallization and ability of GBs mobility as well as local stresses relief at GBs result in the maximum tensile ductility (~50%) at 900 °C.

In further studies, we will focus on devoting to removing the intergranular brittle BCC phases and enhancing coordination deformation ability by tuning the chemical compositions or processing

conditions, such as additive manufacturing[35] and thermal treatment at appropriate temperatures. Moreover, a meaningful exploration under extreme conditions, e.g., dynamic impact and dynamic tension,[36] for this alloy may be one of the burning issues.

Shichao Zhou Thanks Yimin Cui and Zhiran Yan for their help with discussions. This work was supported by the Guangdong Basic and Applied Basic Research Foundation (No. 2019B1515120020), the Fundamental Research Funds for the Central Universities (Grant No. FRF-MP-19-013), the State Key Laboratory for Advanced Metals and Materials (No. 2020-Z08) in the University of Science and Technology Beijing, Mechanism Research and Preparation Technology of High Entropy Alloys with Ultra-high Strength (No. 2020-0531), and the Funds for Creative Research Groups of China (No. 51921001). Peter K. Liaw was supported by the National Science Foundation (Nos. DMR-1611180 and 1809640) and the Army Research Office (Nos. W911NF-13-1-0438 and W911NF-19-2-0049).

DATA AVAILABILITY

The data that support the findings of this study are available within the article.

REFERENCES

[1]*High-Entropy Alloys Fundamentals and Applications*, edited by M. C. Gao, J. W. Yeh, P. K. Liaw, and Y. Zhang (Springer Nature, Switzerland, 2016).
[2]*High-Entropy Materials: A Brief Introduction*, edited by Y. Zhang (Springer Nature Singapore Pte Ltd., Singapore, 2019).
[3]Y. Zhang, T. T. Zuo, Z. Tang, M. C. Gao, K. A. Dahmen, P. K. Liaw, and Z. P. Lu, Prog. Mater. Sci. **61**, 1–93 (2014).
[4]Q. W. Xing, J. Ma, and Y. Zhang, Int. J. Miner., Metall. Mater. **27**, 1379 (2020).
[5]Y. Zhang and R. X. Li, Int. J. Miner., Metall. Mater. **27**, 1309 (2020).
[6]D. Y. Li, C. X. Li, T. Feng, Y. D. Zhang, G. Sha, J. J. Lewandowski, P. K. Liaw, and Y. Zhang, Acta Mater. **123**, 285 (2017).
[7]Y. Zhang, X. H. Yan, W. B. Liao, and K. Zhao, Entropy **20**, e20090624 (2018).
[8]P. J. Shi, R. G. Li, Y. Li, Y. B. Wen, Y. B. Zhong, W. L. Ren, Z. Shen, T. X. Zheng, J. C. Peng, X. Liang, P. F. Hu, N. Min, Y. Zhang, Y. Ren, P. K. Liaw, D. Raabe, and Y. D. Wang, Science **373**, 912 (2021).
[9]N. Xu, S. L. Li, R. G. Li, M. H. Zhang, Z. R. Yan, Y. X. Cao, Z. H. Nie, Y. Ren, and Y. D. Wang, Mater. Sci. Eng.: A **795**, 139936 (2020).
[10]J. Y. He, H. Wang, H. L. Huang, X. D. Xu, M. W. Chen, Y. Wu, X. J. Liu, T. G. Nieh, K. An, and Z. P. Lu, Acta Mater. **102**, 187 (2016).
[11]J. Y. He, H. Wang, Y. Wu, X. J. Liu, H. H. Mao, T. G. Nieh, and Z. P. Lu, Acta Mater. **79**, 41 (2016).
[12]T. Yang, Y. L. Zhao, Y. Tong, Z. B. Jiao, J. Wei, J. X. Cai, X. D. Han, D. Chen, A. Hu, J. J. Kai, K. Lu, Y. Liu, and C. T. Liu, Science **362**, 933 (2018).
[13]Y. J. Liang, L. Wang, Y. Wen, B. Cheng, Q. Wu, T. Cao, Q. Xiao, Y. Xue, G. Sha, Y. Wang, Y. Ren, X. Li, L. Wang, F. Wang, and H. Cai, Nat. Commun. **9**, 4063 (2018).
[14]L. J. Wang, L. Wang, S. C. Zhou, Q. Xiao, Y. Xiao, X. T. Wang, T. Q. Cao, Y. Ren, Y. J. Liang, L. Wang, and Y. F. Xue, Acta Mater. **216**, 117121 (2021).
[15]Y. Tong, D. Chen, B. Han, J. Wang, R. Feng, T. Yang, C. Zhao, Y. L. Zhao, W. Guo, Y. Shimizu, C. T. Liu, P. K. Liaw, K. Inoue, Y. Nagai, A. Hu, and J. J. Kai, Acta Mater. **165**, 228 (2019).
[16]T. Yang, Y. L. Zhao, L. Fan, J. Wei, J. H. Luan, W. H. Liu, C. Wang, Z. B. Jiao, J. J. Kai, and C. T. Liu, Acta Mater. **189**, 47 (2020).
[17]Y. J. Chang and A. C. Yeh, Mater. Chem. Phys. **210**, 111 (2018).
[18]C. M. Kuo and C. W. Tsai, Mater. Chem. Phys. **210**, 103 (2018).
[19]A. A. N. Nemeth, D. J. Crudden, D. E. J. Armstrong, D. M. Collins, K. Li, A. J. Wilkinson, C. R. M. Grovenor, and R. C. Reed, Acta Mater. **126**, 361 (2017).
[20]L. Zheng, G. Schmitz, Y. Meng, R. Chellali, and R. Schlesiger, Crit. Rev. Solid State Mater. Sci. **37**, 181 (2012).
[21]Q. W. Tian, G. J. Zhang, K. X. Yin, L. Wang, W. W. Wang, W. L. Cheng, Y. N. Wang, and J. C. Huang, Intermetallics **119**, 106707 (2020).
[22]B. X. Cao, H. J. Kong, L. Fan, J. H. Luan, Z. B. Jiao, J. J. Kai, T. Yang, and C. T. Liu, Scr. Mater. **194**, 113622 (2021).
[23]J. Z. Ma, W. G. Li, X. H. Zhang, H. B. Kou, J. X. Shao, P. J. Geng, Y. Deng, and D. N. Fang, Mater. Sci. Eng.: A **676**, 165 (2016).
[24]L. Jiang, X. X. Ye, C. Y. Cui, H. F. Huang, B. Leng, Z. J. Li, and X. T. Zhou, Mater. Sci. Eng.: A **668**, 137 (2016).
[25]P. B. Hirsch, Prog. Mater. Sci. **36**, 63 (1992).
[26]A. Suzuki and T. M. Pollock, Acta Mater. **56**, 1288 (2008).
[27]A. Suzuki, G. C. DeNolf, and T. M. Pollock, Scr. Mater. **56**, 385 (2007).
[28]Y. Zhang, J. P. Liu, S. Y. Chen, X. Xie, P. K. Liaw, K. A. Dahmen, J. W. Qiao, and Y. L. Wang, Prog. Mater. Sci. **90**, 358 (2017).
[29]B. B. Zhang, P. K. Liaw, J. Brechtl, J. L. Ren, X. X. Guo, and Y. Zhang, J. Alloys Compd. **820**, 153092 (2020).
[30]H. J. Chung, J. Y. Huh, and W. S. Jung, Mater. Charact. **140**, 9 (2018).
[31]E. X. Pu, W. J. Zheng, Z. G. Song, H. Feng, F. Yang, and H. Dong, Mater. Sci. Eng.: A **699**, 88 (2017).
[32]W. Z. Wang, H. U. Hong, I. S. Kim, B. G. Choi, H. W. Jeong, M. Y. Kim, and C. Y. Jo, Mater. Sci. Eng.: A **523**, 242 (2009).
[33]A. Pandey, F. Kabirian, J. H. Hwang, S. H. Choi, and A. S. Khan, Int. J. Plast. **68**, 111 (2015).
[34]D. A. Woodford, Energy Mater. **1**, 59 (2006).
[35]S. Guan, J. Ren, S. Mooraj, Y. F. Liu, S. Feng, S. B. Zhang, J. Liu, X. S. Fan, P. K. Liaw, and W. Chen, J. Phase Equilib. Diffus. (published online) (2021).
[36]T. W. Zhang, S. G. Ma, D. Zhao, Y. C. Wu, Y. Zhang, Z. H. Wang, and J. W. Qiao, Int. J. Plast. **124**, 226 (2020).